From Far-Field to Near-Field Micro- and Nanoparticle Optical Trapping

applied sciences

MDPI

Review

From Far-Field to Near-Field Micro- and Nanoparticle Optical Trapping

Theodoros D. Bouloumis * and Síle Nic Chormaic *

Light-Matter Interactions for Quantum Technologies Unit, Okinawa Institute of Science and Technology Graduate University, Onna, Okinawa 904-0495, Japan

* Correspondence: theodoros.bouloumis2@oist.jp (T.D.B.); sile.nicchormaic@oist.jp (S.N.C.)

Received: 14 January 2020; Accepted: 14 February 2020; Published: 18 February 2020

Abstract: Optical tweezers are a very well-established technique that have developed into a standard tool for trapping and manipulating micron and submicron particles with great success in the last decades. Although the nature of light enforces restrictions on the minimum particle size that can be efficiently trapped due to Abbe's diffraction limit, scientists have managed to overcome this problem by engineering new devices that exploit near-field effects. Nowadays, metallic nanostructures can be fabricated which, under laser illumination, produce a secondary plasmonic field that does not suffer from the diffraction limit. This advance offers a great improvement in nanoparticle trapping, as it relaxes the trapping requirements compared to conventional optical tweezers although problems may arise due to thermal heating of the metallic nanostructures. This could hinder efficient trapping and damage the trapped object. In this work, we review the fundamentals of conventional optical tweezers, the so-called plasmonic tweezers, and related phenomena. Starting from the conception of the idea by Arthur Ashkin until recent improvements and applications, we present the principles of these techniques along with their limitations. Emphasis in this review is on the successive improvements of the techniques and the innovative aspects that have been devised to overcome some of the main challenges.

Keywords: optical tweezers; optical forces; particle trapping; plasmonics; self-induced back action effect; surface plasmons

1. Introduction

Imagine reducing the size of our fingers by one million times and being able to use them to probe the nanoworld. Now, it is easy to imagine that we could easily capture things of a similar size, such as dielectric nanoparticles, quantum dots with a DNA strand attached to them, proteins and viruses. More than that, we could have the ability to move them in space. In reality, although we cannot modify our fingers in this way, we have found a way to manipulate objects of that size using light!

For more than four centuries, it has been known that light can exert forces on objects [1]. Much later, in 1873, using Maxwell's electromagnetic theory [2], the transfer of momentum from light to illuminated objects was described, resulting in the so-called radiation pressure that leads to objects moving along the direction of light propagation [3]. There were many experiments to follow that confirmed Poynting's calculations, but all of them concluded with the fact that these optical forces were so small that it was difficult even to measure them, let alone utilise them in some meaningful application. In 1936, Beth experimentally demonstrated the transfer of angular momentum from light to a crystal plate and studied the change of polarisation of the beam due to the interaction with matter [4]. However, the birth of lasers in 1960 [5,6] was really what opened new possibilities and topics for research in the field of light-matter interactions.

As the use of lasers became more and more popular in science exploration, Arthur Ashkin, in 1970, experimentally demonstrated how optical radiation forces exerted by lasers can be used to change the motion of dielectric microparticles. He succeeded in trapping them by creating a stable optical potential well [7], thus establishing the new research topic that is known today as optical tweezers.

As always, nature follows its own rules, and soon the primary challenge for optical tweezers became apparent, i.e., the diffraction limit. It seemed to be impossible to focus light beyond the constraints imposed by this limit and, consequently, this created a restriction on the smallest size of particle that could be trapped. Subsequently, the next step in the field's progress was to use surface plasmons excited on metallic nanostructures to confine light into highly intense optical fields, thus enabling superior trapping performance [8]. The first experimental demonstration of trapping using plasmonic structures was reported by Righini et al. [9] in 2007 and, since then, the field of plasmonic optical tweezers started developing rapidly and opened further scientific avenues for investigation. Numerous implementations arose from the research on optical forces and plasmonics and are discussed in further detail elsewhere [10,11]

2. Conventional Optical Tweezers

The Nobel Prize in Physics 2018 was awarded (50%) to Arthur Ashkin "*for the optical tweezers and their application to biological systems*". The whole research field started when Ashkin calculated that "*a power* $P = 1$ *W of cw (continuous wave) argon laser light at* $\lambda = 0.5145$ *μm focussed on a lossless dielectric sphere of radius* $r = \lambda$ *and density* $= 1$ *gm/cc gives a radiation pressure force* $F_{rad} = 2qP/c = 6.6 \times 10^{-5}$ *dyn, where q, the fraction of light effectively reflected back, is assumed to be of order 0.1. The acceleration* $= 1.2 \times 10^8$ *cm/sec*^{2} $\cong 10^5$ *times the acceleration of gravity*" [7]. In SI units, this is equivalent to a radiation pressure force $F_{rad} = 0.66$ nN, leading to an acceleration of 1.2×10^6 m/s^2. In the same work, he demonstrated the first experimental approach to test his calculations on transparent, micron-sized latex spheres in liquids and gas and found that the radiation pressure exerted on the particles from a focussed laser beam was able to accelerate them along the direction of the beam. The measured velocities of the accelerated particles were in very good agreement with the theoretical predictions.

Ashkin next demonstrated trapping of particles using one laser beam and the wall of a glass cell, as well as using two counter-propagating beams with the same characteristics [7]. A few years later, Ashkin et al. [12], reported trapping of dielectric particles (10 μm–25 nm) using a single beam by focussing argon-laser light at 514.5 nm through a high numerical aperture objective lens ($NA = 1.25$). This achievement is attributed to the existence of a force additional to that caused by the radiation pressure (from now on called the scattering force) which originates from the axial beam intensity gradient. It then becomes apparent that, whereas the scattering force depends on the optical intensity and has the direction of the incident beam, the gradient force depends on the intensity gradient and is directed along it from low to high intensities (for the case of particles with higher refractive index than the surrounding medium). Stable optical trapping can occur when these two forces are balanced.

The theoretical mechanism that explains this observation, depends on the relative size of the particle (radius, r) with respect to the wavelength of the laser light (λ). For $r \gg \lambda$, ray optics can be used and the reflection and transmission of the beam from the particle can give rise to the two forces. For $r \ll \lambda$, Rayleigh scattering is assumed and the particle is treated like a dipole in an external electromagnetic field. The two regimes are analysed below, where we assume spherical dielectric particles with refractive index higher than that of the surrounding environment. For the calculation of optical forces acting on particles with arbitrary shapes, the reader is encouraged to study other works [13,14]. Finally, there is an intermediate regime where the particle size is of the same order of magnitude as the wavelength. In this case, the approximations mentioned above cannot be used and, in order to evaluate the forces arising, Maxwell's stress tensor, which relates the interactions between electromagnetic forces and mechanical momentum [10,15], should be used. To handle this complicated mathematical analysis different algorithms have been established, such as the transition matrix (T-matrix) method [16] and the discrete dipole approximation (DDA) [17]. Many works

have followed various approaches for the calculation of the forces in this regime [18–23]. Due to its complexity this regime is not analysed here.

2.1. Ray Optics Approximation ($r \gg \lambda$)

We assume spherical particles of higher refractive index than their surrounding environment, being in a liquid solution and undergoing Brownian motion. As soon as a particle, randomly moving, enters the light beam, a small fraction of light is reflected off the surface of the particle and most of it is refracted on passing through the particle (assuming no absorption). Light carries momentum and, since refraction is a light-matter interaction phenomenon, there is a momentum transfer from the photons to the particle. As known from geometrical optics, the path of the light changes due to refraction, resulting in a change in the momentum ($\vec{p}$) of the photons, over time *(t)*. Obviously, from conservation of momentum for the light-particle system, there should also be a change in the momentum of the particle and this creates a force ($\vec{F}$) acting on the particle, $\vec{F} = d\vec{p}/dt$. To get a first insight, we can initially assume that there is no reflection and the entire beam is refracted inside the sphere as shown in Figure 1a. According to the work done in [24,25], the magnitude of the force on the particle due to the momentum change of a single ray is given by

$$F = \frac{n_m}{c} P, \tag{1}$$

where n_m is the refractive index of the particle, c is the speed of light and P is the power of the incident ray. For a Gaussian beam profile, there is more power towards the centre of the beam than in the tail regions, thus the resultant force from ray 2 (F_2) is stronger than that from ray 1 (F_1), as shown in Figure 1a.

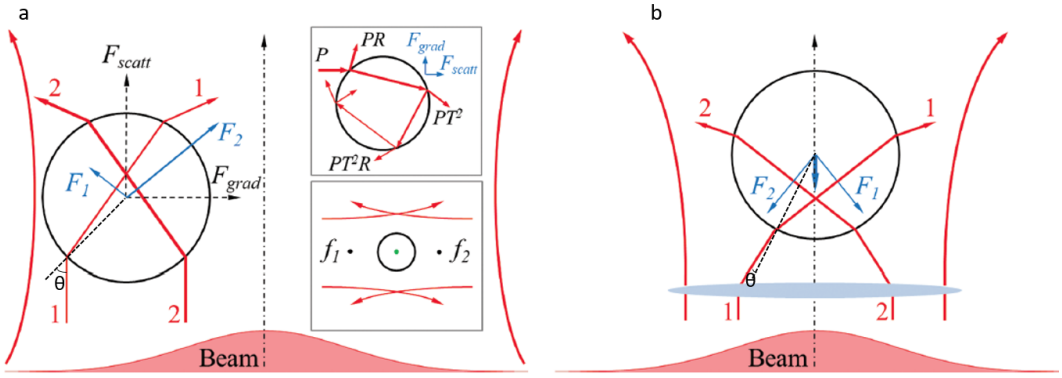

Figure 1. The scattering and gradient forces acting on a dielectric particle in the ray optics regime, arising from a free space (**a**) and a tightly focussed (**b**) Gaussian beam. In the subplot (**a**) the forces push the particle towards the centre of the beam and along the direction of propagation, whereas in (**b**) the forces drag the particle towards the focus of the beam. The upper panel in subplot (**a**) shows the proposed geometry for calculating the forces using Fresnel coefficients. The bottom panel shows trapping using counter-propagating beams with the same characteristics so that the scattering forces cancel each other to achieve a stable trap. Figure reproduced with permission from [26].

The forces acting on the particle can be reduced into a longitudinal component parallel to the incident ray and a transversal one perpendicular to it. As shown in the figure, the longitudinal components of the two forces add up to create a scattering force, whereas the transversal components subtract leading to a gradient force towards the beam's regions of higher intensity. Thence, the particle moves towards the centre of the Gaussian beam and along its axis. Note that, for particles with a lower refractive index than the surroundings, the forces reverse and the particle moves away from the centre of the beam.

If we want to describe the process in a more accurate and mathematically rigorous way, we have to take into account multiple internal reflections and refractions of the rays, as shown in the top inset of Figures 1a and 2. The forces exerted on a particle were first calculated by Roosen [27] by considering Fresnel's reflection (R) and transmission (T) coefficients. For a detailed derivation see [14,28]. The resulting forces are:

$$F_{scat} = F_Z = \sum_{i=1}^{N} \frac{n_m \cdot P_i}{c} \left[1 + R_i \cos(2\theta_i) - \frac{T_i^2[\cos(2\theta_i - 2r_i) + R_i \cos(2\theta_i)]}{1 + R_i^2 + 2R_i \cos(2r_i)} \right] \quad (2)$$

and

$$F_{grad} = F_Y = \sum_{i=1}^{N} \frac{n_m \cdot P_i}{c} \left[R_i \sin(2\theta_i) - \frac{T_i^2[\sin(2\theta_i - 2r_i) + R_i \sin(2\theta_i)]}{1 + R_i^2 + 2R_i \cos(2r_i)} \right], \quad (3)$$

where the sum is over all N rays with power P_i each, interacting with the particle, and θ_i and r_i are the incidence and refraction angles, respectively, as shown in Figure 2. The terms in the square brackets are the dimensionless *trapping efficiencies*, Q_{scat} and Q_{grad}, and account for the efficiency of momentum transfer from the light ray to the particle. We also define the total trapping efficiency of the ray as $Q_{ray} = \sqrt{Q_{scat}^2 + Q_{grad}^2}$. The Fresnel coefficients, R and T, depend on the polarisation of the incident rays. Therefore, the trapping efficiencies and the trapping forces will also be polarisation dependent.

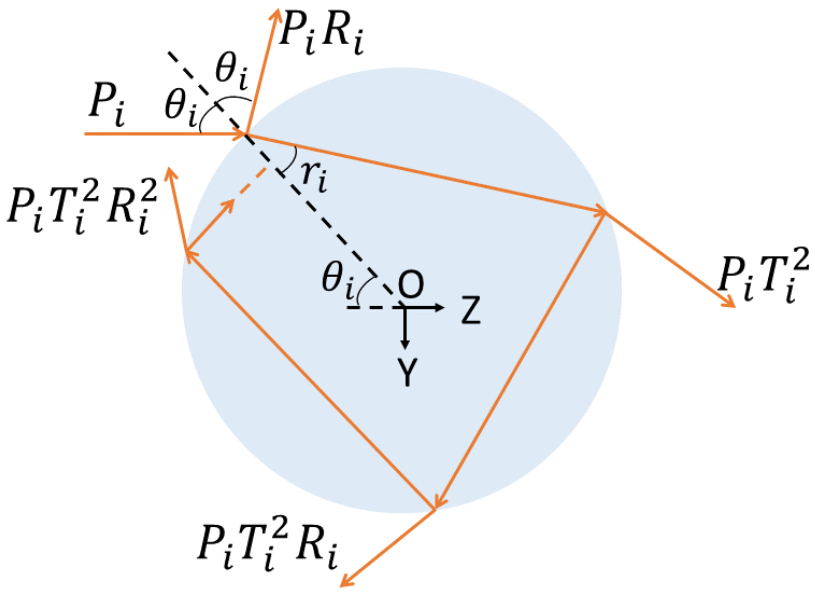

Figure 2. Calculation of the scattering and gradient forces acting on a Mie particle from a single ray, by taking into account geometrical optics and multiple reflection and transmission events, using Fresnel coefficients R and T.

In Figure 3, the trapping efficiencies as a function of the ray's incident angle are plotted for circularly polarised light hitting a glass ($n_m = 1.6$) sphere in water ($n_s = 1.33$). We see that, for incident angles smaller than 70°, the gradient force dominates, but as the incident angle increases, the scattering force becomes significant. This means that, for unfocussed or slightly focussed beams that have a small convergence angle, inevitably most of the rays (taking into account the Gaussian beam profile) will hit the surface of the particle with a large incident angle, θ, as shown in Figure 1a, thereby pushing the particle away. On the contrary, beams that are tightly focussed under a high NA objective lens, cause the rays to hit the surface of the particle with small incident angles (Figure 1b). As a result, the gradient forces strongly dominate over the scattering ones and a stable trap can be established, as Ashkin et al. experimentally demonstrated [12]. Note that, in this case, the longitudinal component of the resulting forces always points towards a location slightly downstream of the beam's focal point,

leading to particle trapping close to, but not exactly at, the focal point. Ashkin's calculations [28] confirmed that, in order to create strong, single-beam traps, high convergence angles are required. For convergence angles smaller than $\sim 30^{\circ}$, single-beam trapping is impossible. Instead, we can use two counter-propagating beams with the same characteristics, as shown in the bottom inset of Figure 1a, to cancel out the scattering forces [7].

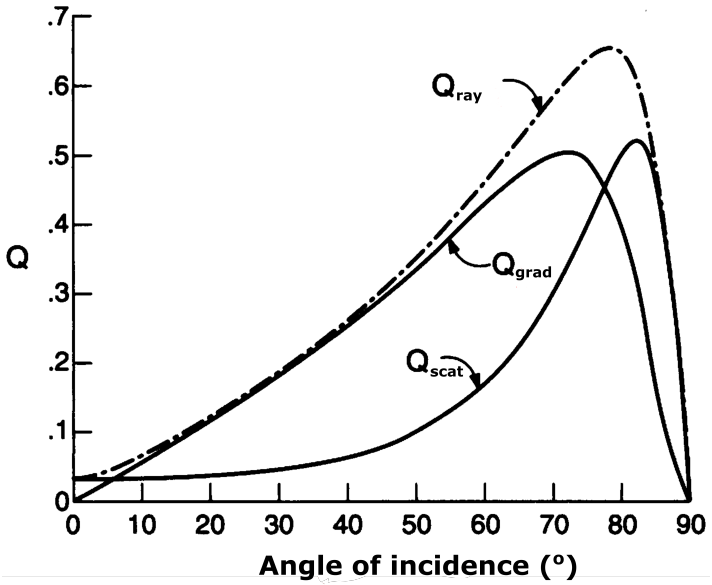

Figure 3. The calculated Q factors for the gradient, scattering, and total trapping efficiencies for a single circularly polarised ray acting on a spherical dielectric particle of effective refractive index $n_{m,eff} = 1.2$, as a function of the incident angle. Figure reproduced with permission from [28].

2.2. Dipole Approximation ($r \ll \lambda$)

In this case, the electric field that the particle experiences is approximately spatially constant over its dimensions, and assuming a dielectric particle, we can treat the entire particle as a collection of induced point dipoles in a homogeneous electric field. Early theoretical work on radiation forces and scattering effects for subwavelength dielectric media can be found in [24,29]. Based on this work and the electromagnetic theory for electromagnetically induced dipoles, we can describe the optical forces and the trapping potential that arises.

The situation for a homogeneous particle can be briefly described as follows (the analysis presented is taken from [14]): The oscillating electromagnetic field from the laser beam causes each of the particle's point dipoles to have a dipole moment

$$\vec{p} = \alpha_0 \vec{E}, \tag{4}$$

where $\vec{E}$ is the electric field and α_0 is the polarizability of the particle, given by the *Clausius-Mossotti relation*

$$\alpha_0 = 4\pi r^3 \epsilon_0 \frac{\epsilon_r - 1}{\epsilon_r + 2}. \tag{5}$$

Here, r is the particle's radius, ϵ_0 is the vacuum dielectric permittivity, and ϵ_r is the particle's dielectric permittivity. The external field causes the dipoles to oscillate and, thus, radiate. Now, we have to take into account the dipole's interaction not only with the external electromagnetic field, but with its own induced scattered field as well. For that reason, the *effective polarizability*, α_d, is introduced as a radiative reaction correction to the intrinsic polarizability of the particle [14] and it is given by

$$\alpha_d = \frac{\alpha_0}{1 - \frac{\epsilon_r - 1}{\epsilon_r + 2}[(k_0 r)^2 + \frac{2i}{3}(k_0 r)^3]}, \tag{6}$$

with k_0 being the vacuum wavenumber and $i = \sqrt{-1}$.

Similarly, in order to calculate the forces acting on all the dipoles, we have to take into account the Lorentz force from the external field and the radiation forces arising from the dipoles themselves. It is also convenient to calculate the time-averaged total force since it is the one that is observable (electromagnetic fields oscillate on the order of $\sim 10^{15}$ Hz which is very fast). Rigorous calculations have been done in [14,26,30]. According to these works, the resulting, time-averaged force acting on a dielectric particle is given by

$$\vec{F} = \frac{1}{4}\alpha_d' \nabla |\vec{E}|^2 + \frac{\sigma_{ext,d}}{c}\vec{S} + \frac{c\epsilon_0 \sigma_{ext,d}}{4\omega i}\nabla \times (\vec{E} \times \vec{E}^*), \tag{7}$$

where α_d' is the real part of the effective polarizability, ω is the angular frequency, $\sigma_{ext,d}$ is the *extinction cross-section*, i.e., the active area of the particle that causes part of the energy of the incident electromagnetic wave to be extinguished due to scattering and absorption from the particle, $\sigma_{ext,d} = \frac{k_0}{\epsilon_0} Im(\alpha_d)$. It, therefore, indicates the rate of energy loss from the incident wave. $\vec{S}$ is the time-averaged real part of the Poynting vector of the incident wave

$$\vec{S} = \frac{1}{2} Re\{\vec{E} \times \vec{H}^*\}. \tag{8}$$

In Equation (7), we see that the force acting on a particle consists of three terms; the third term is called the *spin-curl force* and is related to polarisation gradients in the electromagnetic field that arise when the polarisation is inhomogeneous (e.g., under conditions of tight focussing) [31,32]. The second term is the scattering force pointing in the direction of the Poynting vector, $\vec{S}$, and arises from absorption and scattering phenomena that cause momentum transfer from the field to the particle. The first term is the gradient force and depends on the particle's polarizability and the intensity gradient of the electric field. Since $I = \frac{1}{2} c\epsilon_0 |\vec{E}|^2$, the gradient force can be written as

$$\vec{F}_{grad}(\vec{r}_d) = \frac{1}{2}\frac{\alpha_d'}{c\epsilon_0}\nabla I(\vec{r}_d). \tag{9}$$

From Equation (9) we see that, for particles with positive polarizability (i.e., a higher refractive index than its environment) this force acts towards the direction of the field's higher intensity, i.e., the focal point. At the focal point of a Gaussian beam with a beam waist, w_0, and radial coordinate, ρ, we can approximate the intensity distribution as

$$I(\rho) = I_0 e^{-2\rho^2/w_0^2}, \tag{10}$$

and, for small radial displacements, we can Taylor expand to get

$$I(\rho) \approx I_0 \left(1 - 2\frac{\rho^2}{w_0^2}\right), \tag{11}$$

and substitute into Equation (9). Thence,

$$\vec{F}_{grad}(\vec{r}_d) = \frac{1}{2}\frac{\alpha_d'}{c\epsilon_0}\frac{\partial}{\partial\rho}\left[I_0\left(1 - 2\frac{\rho^2}{w_0^2}\right)\right]\hat{\rho} = -2\frac{\alpha_d'}{c\epsilon_0}\frac{I_0}{w_0^2}\rho\hat{\rho}. \tag{12}$$

By comparing with the restoring force of the classical harmonic oscillator, $\vec{F}(x) = -\kappa x\hat{x}$, we get the trapping constant

$$\kappa_\rho = 2\frac{\alpha'_d}{c\epsilon_0}\frac{I_0}{w_0^2}, \tag{13}$$

and, by integrating Equation (12), we get the trapping potential

$$U(\rho) = \frac{1}{2}\kappa_\rho \rho^2, \tag{14}$$

which is plotted in Figure 4. Note that similar analysis can be used in order to obtain the potential and the trapping constant along the axial direction.

We now consider the main limitation of conventional optical tweezers. Ashkin et al. [12] did some basic calculations and showed that, in order to create a stable optical trap, resisting the Brownian motion of particles in a liquid environment, a potential well as deep as $10k_BT$ is required, where T is the temperature in Kelvin. Although in some cases this is easy to achieve, for subwavelength particles, as they become smaller in size, the gradient force scales down very quickly, making it impossible to satisfy this requirement. By replacing Equation (5) into (6) and simplifying the complex term, we see that $\alpha'_d \propto r^3$, which means that, when the radius of the particle decreases by a factor of 10, the polarizability of the particle and, consequently, the gradient force (Equation (9)) decrease by a factor of 1000. The trapping potential is no longer deep and tight enough to hold the particle (Figure 4) and the trap is inefficient.

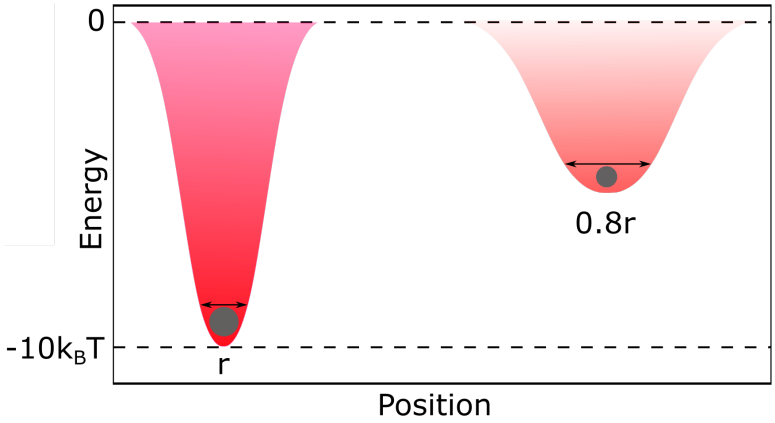

Figure 4. Graphical representation of the trapping potential wells for a polystyrene bead of radius r and $0.8r$. A small decrease in the particle's size creates a significantly shallower and broader trapping potential well, which offers much weaker confinement and, thus, the particle has a higher probability to escape from the trap.

Equations (5), (6) and (13) can be used to calculate the change in the trapping stiffness if the particle has a radius of $0.8r$:

$$\Delta\kappa = \frac{\kappa_{0.8r} - \kappa_r}{\kappa_r} = \frac{\alpha'_{d0.8r} - \alpha'_{dr}}{\alpha'_{dr}}. \tag{15}$$

Calculations show that for $r = 100$ nm, there is a 53% decrease in the trapping stiffness when the particle's radius decreases to $0.8r$. From Equation (13) we see that, in order to compensate for this effect and increase the trapping constant and the gradient force, we can either increase the intensity of the incident field (I_0) or focus tighter (w_0). However, even though in some cases it is experimentally possible to increase the intensity of the field by a factor of 1,000, the heat accumulation will be very large and could eventually destroy the particle, in particular if it is a biological sample. On the other hand, the diffraction limit allows for focussing of the beam to a diameter of approximately half of its wavelength, thus creating a certain minimum value for w_0 (see Equation (13)). Additionally, as the

particle becomes smaller, the viscous drag reduces and the particle's Brownian motion increases and escape from the trap is more likely [11].

All the above highlighted issues contribute to a number of limitations for the use of conventional optical tweezers in particle manipulation. As a result, an alternative approach was established that relies on surface plasmons and was based on the observations of moving particles in evanescent fields.

3. Plasmonic Optical Tweezers

Recent advances in the fields of optics and nano-optics have helped to overcome the diffraction limit problem by using evanescent fields instead of propagating ones; these have the intrinsic property of confinement beyond the diffraction limit. A detailed analysis can be found in [33,34]. The current trend is to use metallic nanostructures (see [35] for a recent review on different platforms) in which surface plasmons can be excited at resonant frequencies and that concentrate the electric field to create highly intense fields, thereby significantly increasing the trapping potential depth that a nanoparticle may experience.

In 1992, Kawata et al. demonstrated the motion of microparticles under illumination from evanescent fields [36] and they were soon followed by Prieve et al. [37]. Some years later, in 1997, Novotny et al. theoretically proposed and calculated optical trapping at the nanoscale, using enhanced evanescent fields from a laser-illuminated metallic nanotip [8]. Okamoto et al., at around the same time, did similar work, but used a metallic nano-aperture instead of a tip [38]. Figure 5 shows their proposed geometrical model. Analytical work on the calculation of forces acting on a dielectric sphere from an evanescent field can also be found in [39].

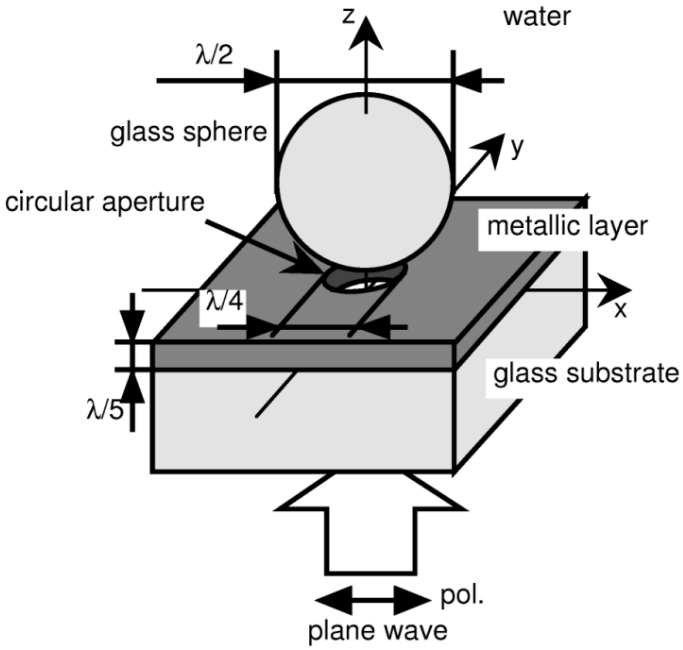

Figure 5. The geometrical model, studied by Okamoto et al., for subwavelength particle trapping, utilising the evanescent field near a metallic nano-aperture. This is the most commonly studied and reported geometry due to its simplicity to fabricate using the focussed ion beam (FIB) milling technique. Figure reproduced with permission from [38].

The advantage of using this kind of configuration comes from the fact that the incident field no longer directly creates the trapping potential, but rather excites the surface plasmons (SP) on the metal/dielectric interface. The SPs, in turn, create the strong evanescent field that provides the trapping potential. The main benefit of trapping using an evanescent field is that, by nature, it has

a very high field gradient, thus exerting a large trapping force (see Equation (9)) with no need to increase the incident intensity, thereby leading to a reduction of radiation damage to the sample. In other words, superior trapping conditions can be achieved with much lower illumination power compared to conventional optical tweezers.

It was then just a matter of time for plasmonic optical tweezers to be realised. In 2007, Righini et al., using a geometry of total internal reflection similar to the one shown in Figure 6a, and a pattern consisting of 4.8 μm-diameter gold discs fabricated on glass, performed multiple trapping of 4.88 μm polystyrene colloids [9]. Note that the laser beam was unfocussed, with a waist of about 100 μm and the intensity was more than 10 times lower than that required for conventional optical tweezers with similar characteristics. Theoretical work had been done earlier in order to study the forces arising in such a configuration [40]. Also, in earlier experimental work, the authors used a photonic force microscope to measure the plasmon radiation forces acting on polystyrene beads at the localised surface plasmon resonance. They reported forces 40 times stronger than those obtained in the absence of SP excitation [41].

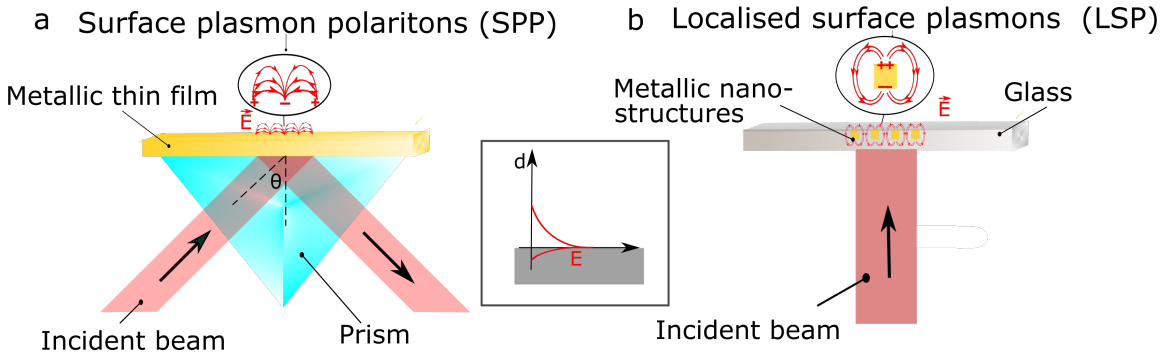

Figure 6. (**a**) Schematic of the Kretschmann configuration [42,43] used to excite the surface plasmon polaritons (SPP). Light is coupled into SPPs under total internal reflection in order to compensate for the light momentum mismatch. The angle of incidence, θ, controls both the scattering and the gradient forces, allowing for tuning of the total trapping force. (**b**) Excitation of the localised surface plasmons (LSP) can happen under direct illumination of the metallic nanostuctures. The geometrical characteristics of the nanostructures on the metallic thin film define the resonance frequency and the forces that arise from the plasmonic field. Inset shows the exponential decay of the evanescent plasmonic field from the surface of the material.

It is important to mention the two distinct types of surface plasmons. Surface plasmon polaritons (SPP) are propagating electromagnetic surface waves that appear at the metal/dielectric interface due to the motion of the metal's free electrons driven by the incident electromagnetic field. They are evanescent modes and, thus, they produce localised fields with a high intensity decaying exponentially away from the metal surface. Due to the very large intensity gradient, they exert strong gradient forces on the trapped particles (see Equation (9)), thereby producing stable traps. However, because SPPs are pure evanescent modes, direct coupling to propagating light is not possible and, in order to excite them, a different geometrical approach is required. The most common experimental method relies on the Kretschmann configuration [42,43], which is shown in Figure 6a. Light is coupled into SPPs under total internal reflection in order to compensate for the light momentum mismatch. The crucial parameter in this configuration is the angle of incidence, θ, which controls both the scattering and the gradient force, allowing for tuning of the total trapping force.

In contrast, localised surface plasmons (LSP) are related to the bound electrons that are present near to nano-apertures or nanoparticles much smaller than the wavelength of the electromagnetic field. Bound electrons are susceptible to a damping oscillation due to the nucleus attraction and, as a result, they have a characteristic resonance frequency, unlike SPPs that can be excited over a wide range of frequencies. The benefits of LSPs are that they can directly couple to propagating light and their resonance frequency can be tuned by changing the size and the shape of the nano-aperture/nanoparticle (Figure 6b). In a theoretical work done on LSPs, the dramatic dependence of the strength of the excited evanescent field on the frequency of the incident electromagnetic field was presented [40]. Detailed mathematical analysis on the excitation of surface plasmons and the forces arising can be found in Ref. [14,44].

To date, many different configurations have been reported using SPs for efficient trapping of subwavelength particles, such as plasmonic nanodots [45], nano-antennas [46], nanocavities [47] and nano-apertures of different shapes and sizes [48,49], relying on very low incident power. Note that, in these cases, rigorous calculations need to be done beforehand in order to determine crucial parameters such as resonance wavelength and polarisation in compliance with the plasmonic field excitation requirements. Additionally, the fabrication of such nanostructures can also be a challenging task. The most popular techniques to fabricate structures of these sizes is focussed ion beam (FIB) milling and electron beam lithography (EBL), with a resolution of about 10 nm. With these considerations, the implementation of plasmonic optical tweezers can, overall, be relatively time consuming.

The main disadvantage with plasmonic structures is the conductive nature of metals, which is linked to heat induction and dissipation to the surrounding environment. The excitation of the LSP leads to a frequency-dependent absorption of light by the structures in the metallic thin film, which provides maximum absorption for maximum plasmonic field intensity. The dynamic behaviour of the nanoparticles in and around the optical potential well can be strongly affected by the resultant photothermal effects and various studies have investigated this phenomenon [50,51]. Methods to suppress the heat dissipation have been proposed [52,53] and these could be applied in a synergistic way to mitigate the problem. Additionally, controlled fabrication of the plasmonic structures could enable researchers to take advantage of the self-induced back action effect [54] (see below).

Self-Induced Back Action Effect

The diffraction and transmission of light through a single, subwavelength-sized circular hole on a metallic surface was first theoretically studied in 1944 by Bethe [55]. Assuming a perfectly conducting and infinitely thin material, Bethe calculated that the transmitted light would scale as $T \propto (d/\lambda)^4$, where d is the radius of the hole and λ the wavelength of the incident light, as illustrated in Figure 7. In 1998, the remarkable phenomenon of the *extraordinary transmission of light* was experimentally observed by Ebbesen et al. [56], when they studied the effects of the geometrical characteristics of an array of tiny holes, drilled on different metallic films, on the transmission of light. In that work, UV-Vis-NIR spectrophotometry of the array was performed and it revealed the existence of maxima in the transmission intensity, see Figure 8a, with much higher values than predicted from Bethe's theory. These maxima could not be explained simply by diffraction theory and they were associated with the resonant frequencies of the excited surface plasmons of the metal. A detailed theoretical explanation of this observation was provided a few years later [57,58], where the calculated positions of the transmission maxima were in very good agreement with the experiment, confirming that the mechanism of extraordinary transmission was taken into account in their model (Figure 8b).

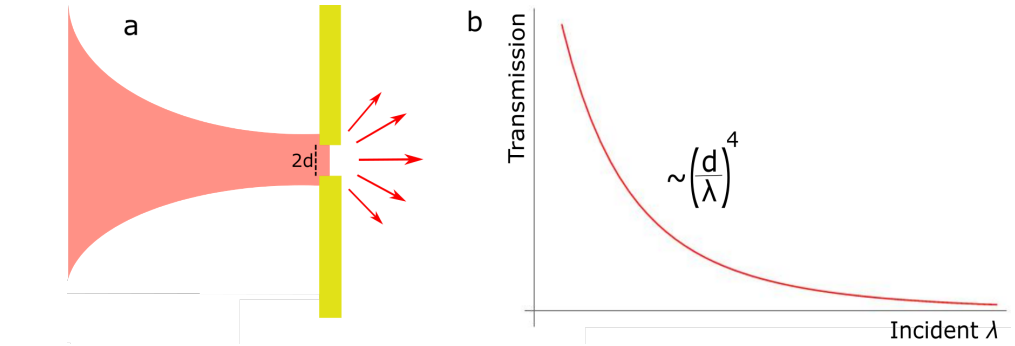

Figure 7. (**a**) Diffraction and transmission of visible light through a subwavelength circular hole of radius, d, on a perfectly conducting and infinitely thin metallic film. (**b**) According to Bethe's calculation the transmission of incident light λ scales as $(d/\lambda)^4$. Figure inspired by [59].

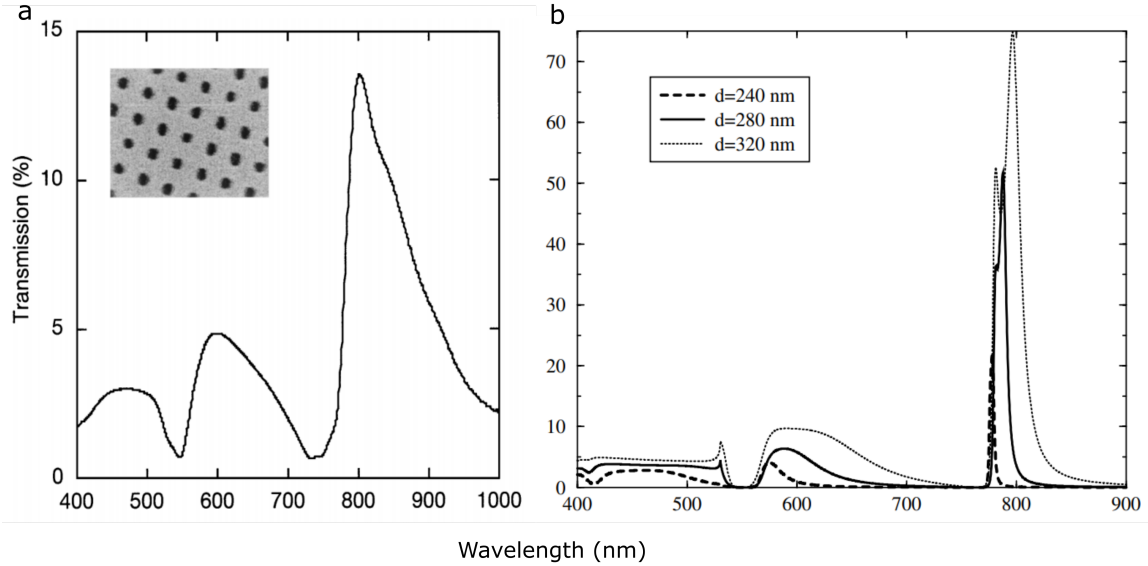

Figure 8. (**a**) Experimental and (**b**) theoretical plots of the normalised transmittance as a function of the incident light wavelength, for a square array of holes on a Ag thin film with thickness h =320 nm. The diameter of the holes was d = 280 nm in the experiment and d = 240, 280, 320 nm for the calculations and the lattice constant 750 nm. Inset in the left plot shows an SEM image of the nano-hole lattice. Image reproduced with permission from [57].

In addition, in his theoretical work, Abajo investigated the case whereby the nano-hole is filled with a dielectric material of high refractive index (Si). He found that the transmission cross-section at the resonance frequency was almost three times higher than without the filling, leading to increased transmission [58]. The increase of the refractive index at the nano-hole causes the wavelength of the light to decrease:

$$n_{fill} = \frac{c}{c_{fill}} > 1 \Leftrightarrow n_{fill} = \frac{\lambda}{\lambda_{fill}} > 1 \Leftrightarrow \lambda_{fill} < \lambda. \tag{16}$$

A consequence of this effect is that, according to Bethe's theory, the transmission of light through the subwavelength aperture increases, a phenomenon also known as dielectric loading. Figure 9 shows how the wavelength shift causes a significant increase in the transmission of light T_2, compared to transmission of light T_1 through a non-filled aperture.

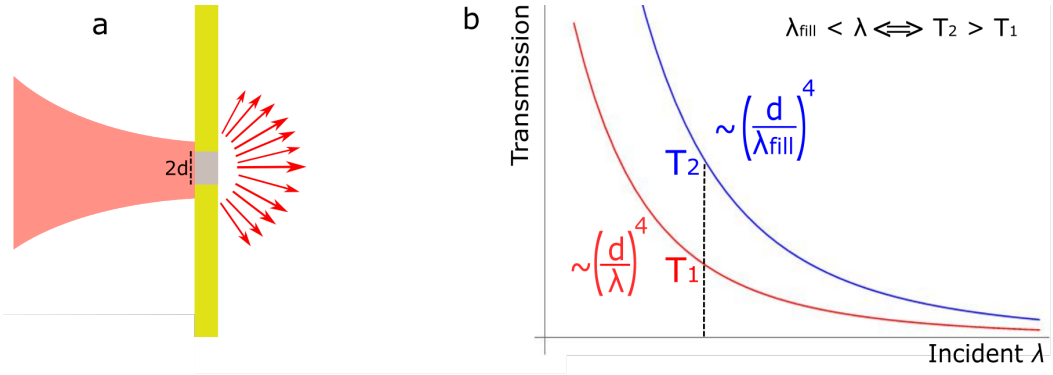

Figure 9. (**a**) The presence of a dielectric material of higher refractive index than the surroundings causes an increase in the transmission of light through the subwavelength aperture. (**b**) Shift of the transmission line due to existence of the dielectric material, leading to higher transmission T_2, compared to the transmission of light T_1 in the case of non-filling. Figure inspired by [59].

As mentioned in the previous section, at around the same time, the use of plasmonics for enhanced optical trapping had started to attract attention and, despite how promising they might seem for trapping subwavelength particles, it became apparent that their use is limited to particles with a minimum diameter around 100 nm due to photothermal effects [60].

It was the combination of these two different studies on plasmonics that brought the realisation that the resonance frequency of the excited plasmonic field is very sensitive to changes of the local refractive index. Thus, by proper engineering of the plasmonic structure, the trapped particle itself could actively contribute to its own trapping potential in a dynamical way [61]. This plasmonic structure - particle interaction promised high tunability of the trapping potential, which was no longer a static. This gave rise to the *self-induced back action* (SIBA) effect and the first experimental trapping utilising this effect, where polystyrene spheres of 100 and 50 nm size were successfully trapped with incident powers as low as 0.7 and 1.9 mW, respectively [54], pushing further the boundaries of plasmonic nanotweezers.

A comprehensive mathematical analysis of the SIBA effect has been done by Neumeier et al. [62], for a small dielectric particle trapped in a plasmonic nanocavity. They demonstrated the additional restoring forces that act on the particle as it tries to escape from the trap. Below, we present the basic principle of the SIBA effect following the analysis done in [60].

The gradient force experienced by a nanosphere with radius $r \ll \lambda$ of the incident light, is given by Equation (9), as mentioned previously. If we assume small displacements of the particle from the centre of the trap ($|x| \ll \lambda$), then according to the overdamped Langevin equation the particle's motion inside the trap is given by

$$\gamma \dot{x}(t) + \kappa_{tot} x(t) = \xi(t), \tag{17}$$

where γ is the viscous damping [63], assuming that the particle exists in a liquid environment, κ_{tot} is the stiffness of the trap, indicating how strongly the particle is confined in the trap, and ξ represents thermal fluctuations [64]. Due to their strong interaction there is a dispersive coupling between the cavity and the particle. Thus, the motion of the particle in the trap causes the plasmon resonance frequency of the cavity to shift by $\delta\omega_0(x_p)$, where x_p indicates the frequency dependence on the particle's position. Then, for a cavity with mode volume, V_m, and intensity profile, $f(x_p)$, normalised to 1 for maximum intensity, the perturbation theory for shifts much smaller than the cavity eigenfrequency, ω_c, yields [65]

$$\delta\omega_0(x_p) = \omega_c \frac{\alpha_d}{2V_m\epsilon_0} f(x_p), \tag{18}$$

with α_d being the effective polarizability, from Equation (6). Note that the magnitude of the shift strongly depends on the relative size of the particle and the cavity and, as expected from Equation (18),

a decrease in the particle's size (decrease in α_d, see Equations (5) and (6)), decreases the magnitude of the shift [66].

Now, for incident laser frequency, ω, and $\Delta \equiv \omega - \omega_c$ being the cavity detuning, the intracavity intensity, $I(\omega)$, is given, on Taylor expansion, as

$$I(\omega) = I_0 \frac{(\Gamma/2)^2}{(\Delta - \delta\omega_0)^2 + (\Gamma/2)^2} \approx I_{opt} - \frac{2\delta\omega_0(x_p)\Delta}{\Delta^2 + (\Gamma/2)^2} I_{opt} + ... \tag{19}$$

where Γ is the cavity linewidth and $I_{opt} = I_0 \frac{(\Gamma/2)^2}{\Delta^2 + (\Gamma/2)^2}$ is the empty cavity profile.

As can been seen from Equation (19), the intensity of light inside the cavity, to a first order approximation, is given by the term related to the intensity of the empty cavity, plus the one related to the frequency shift caused by the presence of the particle. This second term is the one that causes the SIBA effect and modifies the optical potential. Following Equation (19), we can also write the total trapping stiffness, κ_{tot}, as [62]

$$\kappa_{tot} = \kappa_{opt} + \kappa_{SIBA}, \tag{20}$$

where κ_{opt} is constant and depends on the cavity resonance profile and κ_{SIBA} is a function of the particle's displacement. According to Neumeier et al., in order to optimise κ_{SIBA}, the cavity has to be constructed such that the *back-action parameter*, $\upsilon = \delta\omega_0(x_p)/\Gamma$, is maximised [62]. This means that, while the particle is trapped in the centre of the trap, the resonance shift is such that the photon flux from the cavity is less than the maximum possible. As a consequence, when the particle moves away from the centre of the trap, the resonance shift causes the photon flux to increase and, thus, the intensity of the transmitted light increases. From Equation (9) an increase to the intensity leads to an increase to the gradient force, which restores the particle back to the centre of the trap. Then, the photon flux and the intensity decrease and, again, the particle tends to move away from the trap centre. This kind of feedback is referred to as *"optomechanical coupling"* because there is a continuous response between light and mechanical motion. The field of optomechanics in plasmonics is rather unexplored and, to our knowledge, there is only one work that reports an optomechanical coupling constant [60]. This optomechanical coupling not only relaxes the requirements for high power trapping, but also prevents the sample from overheating since most of the time the particle is trapped using a low intensity. It remains open to exploration to find ways to increase the optomechanical coupling constant and to achieve even higher particle confinement and motion transduction.

In Figure 10a, the vertical dashed line represents the excitation laser wavelength, the black lineshape is the empty cavity mode resonance, and the orange is the shifted one due to particle trapping. In the first case (Figure 10(ai), blue-shifted) the cavity resonance is set to be blue-detuned from the excitation laser, such that when the particle is trapped, the resonance red-shift increases the photon flux to the maximum value and the gradient force reaches a maximum. However, when the particle moves away from the centre of the trap, the lineshape blue shifts towards the empty cavity resonance and the intensity decreases. In order to increase the gradient force, the power of the laser has to, externally, be increased, thus, it is not the most efficient scenario for trapping. In the case where the empty mode resonance is slightly blue-detuned (Figure 10(aii), resonance), the red-shifting due to a trapping event creates a symmetrical lineshape around the laser wavelength. As the particle tries to escape from the trap, the resonance moves towards the empty mode value and causes an increase in the photon flux and the light intensity of light, thus increasing the gradient force. Finally, in the case where the empty cavity resonance is designed to be red-detuned from the excitation laser (Figure 10(aiii), red-shifted), the trapped object further red-shifts the resonance, leading to significant reduction in the intensity and the gradient force. In this configuration, the trapping becomes very inefficient and an increase to the laser power is necessary to keep the particle in the trap.

The intensity required to keep the particle efficiently in the trap is less in the second case where the SIBA effect contributes to an increase in the total trapping stiffness. This was also experimentally

observed for the first time by Mestres et al. [60]. Figure 10b shows the experimental data that confirm the superior trapping efficiency of a plasmonic cavity, designed to be slightly blue-detuned from the excitation wavelength (Figure 10(aii,bii)). The remarkable effect of SIBA is now apparent and, by proper design of the plasmonic structure, we can have a larger trapping stiffness at a lower laser power, thereby reducing heat transfer to the specimen.

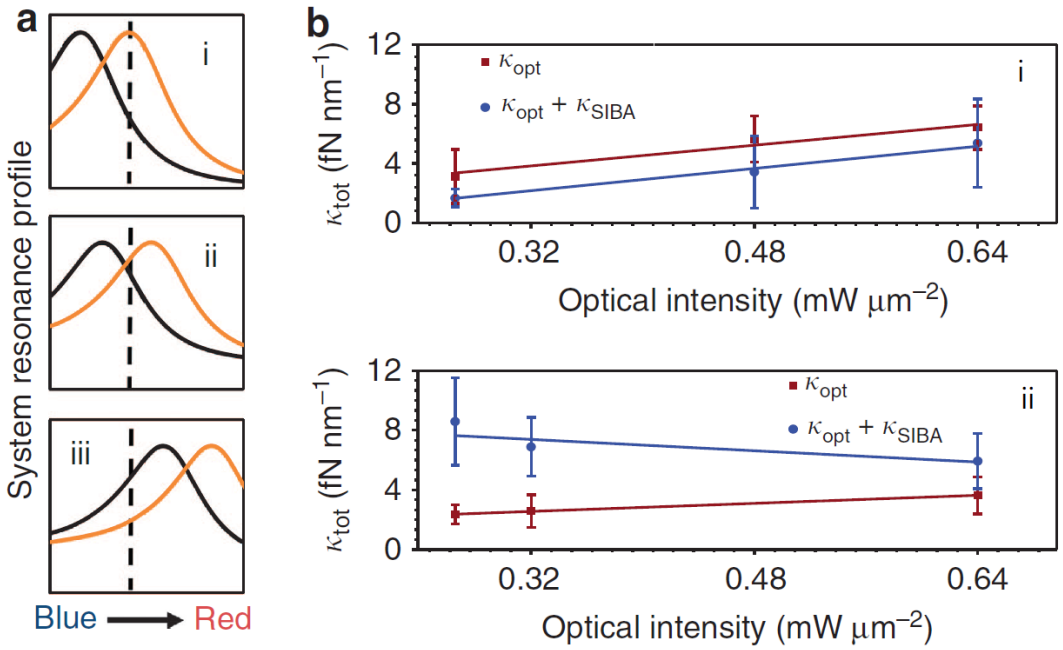

Figure 10. (**a**) Three different cases of the resonance profile of a plasmonic cavity (black line). In case (i), (ii), and (iii) the cavity is designed to be blue-detuned, slightly blue-detuned and red-detuned, respectively, from the excitation laser (vertical dashed line). The orange line represents the frequency shift of the resonance of the cavity due to the existence of the particle near by it. In case (ii), the SIBA effect has a positive influence on the trap and, whenever the particle tries to escape, the photon flux (intensity) increases, which causes, increase to the gradient force. (**b**) Experimental measurements of the total trapping stiffness as a function of the incident laser intensity. (**b**)(i) corresponds to case (**a**)(i), where as the intensity decreases both the total and the empty cavity trapping stiffness decrease, making the trap inefficient. (**b**)(ii) corresponds to case (**a**)(ii), and clearly shows that, as the laser intensity decreases, the empty cavity trapping stiffness decreases, but the total stiffness increases due to the positive contribution from the SIBA effect, thus achieving a stable, self-adjustable trap. Figures reproduced from [60], under Creative Commons license: CC BY-NC-ND 4.0 https://creativecommons.org/licenses/by-nc-nd/4.0/.

4. Conclusions and Future Perspectives

It is interesting to see how a relatively basic idea can be transformed into a very useful technique for manipulating matter, finally leading to the awarding of a Nobel Prize in Physics. Optical tweezers, whether conventional or plasmonic, are now widely used in many fields of research, due to such scientific efforts. A big advantage of optical tweezers is that they are relatively easy and inexpensive to build or to modify according to research needs. Thus, they have found application in various fields such as physics [67], biosciences [68–70], and chemistry [71]. In many cases, they serve as a tool to trap or manipulate matter while simultaneously making other measurements, such as Raman spectroscopy of biological samples [72–74]. There is also an increased interest in exploring the area between particle trapping and atom cooling to study quantum phenomena at the mesoscopic scale [75,76], indicating that optical tweezers may even impact the development of quantum-based technologies. Very recently, ground state laser cooling of a subwavelength sized dielectric particle

trapped in an optical tweezers has been reported [77], providing a route to explore topics such as quantum sensing using macrosystems, so it is certainly a very exciting time for further advances in the field.

Of course, there are many open questions and challenges to overcome in order to optimise the techniques so that they can be used to efficiently trap not only particles in the range of less than 10 nm, but also biological samples such as proteins, viruses and DNA for which the treatment as a spherical dielectric particles is inadequate. Although not discussed here, the geometrical shape and material of the trapped object play a significant role in the trapping conditions and, in particular for biomaterials, heating and rapid temperature changes must be taken into consideration. One of the biggest challenges for progress in optical trapping is the ability to fully control and manipulate many trapped nano-objects simultaneously. While this has been achieved for micro-objects by using modulation of the light field, it has yet to be realized in the nanoscale. We can expect to see this barrier surmounted in the near future.

Funding: This research received no external funding.

Acknowledgments: The authors would like to thank Okinawa Institute of Science and Technology Graduate University for funding, and D. G. Kotsifaki, P. Reece, Y. Okada, F. Pauly, and G. Tkachenko for constructive comments.

Conflicts of Interest: The authors declare no conflict of interest.

References

1. Kepler, J. *De Cometis Libelli Tres*; Typis Andreæ Apergeri, sumptibus Sebastiani Mylii bibliopolæ Augustani; Augustae Vindelicorum: Augsburg, Germany, 1619.
2. Maxwell, J. *A Treatise on Electricity and Magnetism*; Clarendon Press: Oxford, UK, 1873; Volume 2.
3. Poynting, J.H.; William, S.J. On the transfer of energy in the electromagnetic field. *Philos. Trans. R. Soc.* **1884**, *175*. [CrossRef]
4. Beth, R.A. Mechanical Detection and Measurement of the Angular Momentum of Light. *Phys. Rev.* **1936**, *50*, 115–125, doi:10.1103/PhysRev.50.115. [CrossRef]
5. Maiman, T.H. Stimulated Optical Radiation in Ruby. *Nature* **1960**, *187*, 493–494, doi:10.1038/187493a0. [CrossRef]
6. Schawlow, A.L.; Townes, C.H. Infrared and Optical Masers. *Phys. Rev.* **1958**, *112*, 1940–1949, doi:10.1103/PhysRev.112.1940. [CrossRef]
7. Ashkin, A. Acceleration and trapping of particles by radiation pessure. *Phys. Rev. Lett.* **1970**, *24*, 156–159, doi:10.1103/PhysRevLett.24.156. [CrossRef]
8. Novotny, L.; Bian, R.X.; Xie, X.S. Theory of nanometric optical tweezers. *Phys. Rev. Lett.* **1997**, *79*, 645–648, doi:10.1103/PhysRevLett.79.645. [CrossRef]
9. Righini, M.; Zelenina, A.S.; Girard, C.; Quidant, R. Parallel and selective trapping in a patterned plasmonic landscape. *Nat. Photonics* **2007**, *3*, 477–480, doi:10.1038/nphys624. [CrossRef]
10. Marago, O.M.; Jones, P.H.; Gucciardi, P.G.; Volpe, G.; Ferrari, A.C. Optical trapping and manipulation of nanostructures. *Nat. Nanotechnol.* **2013**, *8*, 807–819, doi:10.1038/nnano.2013.208. [CrossRef]
11. Juan, M.L.; Righini, M.; Quidant, R. Plasmon nano-optical tweezers. *Nat. Photonics* **2011**, *5*, 349–356, doi:10.1038/nphoton.2011.56. [CrossRef]
12. Ashkin, A.; Dziedzic, J.M.; Bjorkholm, J.E.; Chu, S. Observation of a single-beam gradient force optical trap for dielectric particles. *Opt. Lett.* **1986**, *11*, 288–290, doi:10.1364/OL.11.000288. [CrossRef]
13. Ling, L.; Zhou, F.; Huang, L.; Li, Z.Y. Optical forces on arbitrary shaped particles in optical tweezers. *J. Appl. Phys.* **2010**, *108*, 073110, doi:10.1063/1.3484045. [CrossRef]
14. Jones, P.; Marago, O.M.; Volpe, G. *Optical Tweezers: Principles & Applications*; Cambridge University Press: Cambridge, UK, 2015.
15. Pfeifer, R.N.C.; Nieminen, T.A.; Heckenberg, N.R.; Rubinsztein-Dunlop, H. Colloquium: Momentum of an electromagnetic wave in dielectric media. *Rev. Mod. Phys.* **2007**, *79*, 1197–1216, doi:10.1103/RevModPhys.79.1197. [CrossRef]

16. Borghese, F.; Denti, P.; Saija, R. *Scattering from Model Nonspherical Particles*; Springer: Berlin/Heidelberg, Germany, 2007. doi:10.1007/978-3-540-37414-5. [CrossRef]
17. Draine, B.T.; Flatau, P.J. Discrete-dipole approximation for scattering calculations. *J. Opt. Soc. Am. A* **1994**, *11*, 1491–1499, doi:10.1364/JOSAA.11.001491. [CrossRef]
18. Ranha Neves, A.A.; Cesar, C.L. Analytical calculation of optical forces on spherical particles in optical tweezers: Tutorial. *J. Opt. Soc. Am. B* **2019**, *36*, doi:10.1364/josab.36.001525. [CrossRef]
19. Lock, J.A. Calculation of the radiation trapping force for laser tweezers by use of generalized Lorenz-Mie theory. I. Localized model description of an on-axis tightly focused laser beam with spherical aberration. *Appl. Opt.* **2004**, *43*, 2532–2544, doi:10.1364/AO.43.002532. [CrossRef]
20. Lock, J.A. Calculation of the radiation trapping force for laser tweezers by use of generalized Lorenz-Mie theory. II. On-axis trapping force. *Appl. Opt.* **2004**, *43*, 2545–2554, doi:10.1364/AO.43.002545. [CrossRef]
21. Rohrbach, A.; Stelzer, E.H.K. Optical trapping of dielectric particles in arbitrary fields. *J. Opt. Soc. Am. A* **2001**, *18*, 839–853, doi:10.1364/JOSAA.18.000839. [CrossRef]
22. Ren, K.F.; Gréha, G.; Gouesbet, G. Radiation pressure forces exerted on a particle arbitrarily located in a Gaussian beam by using the generalized Lorenz-Mie theory, and associated resonance effects. *Opt. Commun.* **1994**, *108*, 343–354, doi:https://doi.org/10.1016/0030-4018(94)90673-4. [CrossRef]
23. Barton, J.P.; Alexander, D.R.; Schaub, S.A. Theoretical determination of net radiation force and torque for a spherical particle illuminated by a focused laser beam. *J. Appl. Phys.* **1989**, *66*, 4594–4602, doi:10.1063/1.343813. [CrossRef]
24. Gordon, J.P. Radiation forces and momenta in dielectric media. *Phys. Rev. A* **1973**, *8*, 14–21, doi:10.1103/PhysRevA.8.14. [CrossRef]
25. Ashkin, A.; Dziedzic, J.M. Radiation pressure on a free liquid surface. *Phys. Rev. Lett.* **1973**, *30*, 139–142, doi:10.1103/PhysRevLett.30.139. [CrossRef]
26. Bradac, C. Nanoscale optical trapping: A review. *Adv. Opt. Mater.* **2018**, *6*, doi:10.1002/adom.201800005. [CrossRef]
27. Roosen, G. La lévitation optique de sphères. *Can. J. Phys.* **1979**, *57*, 1260–1279, doi:10.1139/p79-175. [CrossRef]
28. Ashkin, A. Forces of a single-beam gradient laser trap on a dielectric sphere in the ray optics regime. *Biophys. J.* **1992**, *61*, 569–582, doi:10.1016/S0006-3495(92)81860-X. [CrossRef]
29. Purcell, E.M.; Pennypacker, C.R. Scattering and absorption of light by nonspherical dielectric grains. *Astrophys. J.* **1973**, *186*, 705–714, doi:10.1086/152538. [CrossRef]
30. Spesyvtseva, S.E.S.; Dholakia, K. Trapping in a material world. *ACS Photonics* **2016**, *3*, 719–736, doi:10.1021/acsphotonics.6b00023. [CrossRef]
31. Iglesias, I.; Sáenz, J.J. Scattering forces in the focal volume of high numerical aperture microscope objectives. *Opt. Commun.* **2011**, *284*, 2430–2436, doi:10.1016/j.optcom.2011.01.029. [CrossRef]
32. Gu, M. Imaging with a High Numerical-Aperture Objective. In *Advanced Optical Imaging Theory*; Springer: Berlin/Heidelberg, Germany, 2000; pp. 143–176, doi:10.1007/978-3-540-48471-4_6. [CrossRef]
33. Vigoureux, J.M.; Courjon, D. Detection of nonradiative fields in light of the Heisenberg uncertainty principle and the Rayleigh criterion. *Appl. Opt.* **1992**, *31*, 3170–3177, doi:10.1364/AO.31.003170. [CrossRef]
34. Novotny, L.; Hecht, B. *Principles of Nano-Optics*; Cambridge University Press: Cambridge, UK, 2012.
35. Kotsifaki, D.; Nic Chormaic, S. Plasmonic optical tweezers based on nanostructures: fundamentals, advances and prospect. *Nanophotonics* **2019**, *8*, 1227–1245, doi:10.1515/nanoph-2019-0151. [CrossRef]
36. Kawata, S.; Sugiura, T. Movement of micrometer-sized particles in the evanescent field of a laser beam. *Opt. Lett.* **1992**, *17*, 772–774, doi:10.1364/OL.17.000772. [CrossRef]
37. Prieve, D.C.; Walz, J.Y. Scattering of an evanescent surface wave by a microscopic dielectric sphere. *Appl. Opt.* **1993**, *32*, 1629–1641, doi:10.1364/AO.32.001629. [CrossRef] [PubMed]
38. Okamoto, K.; Kawata, S. Radiation force exerted on subwavelength particles near a nanoaperture. *Phys. Rev. Lett.* **1999**, *83*, 4534–4537, doi:10.1103/PhysRevLett.83.4534. [CrossRef]
39. Walz, J.Y. Ray optics calculation of the radiation forces exerted on a dielectric sphere in an evanescent field. *Appl. Opt.* **1999**, *38*, 5319–5330, doi:10.1364/AO.38.005319. [CrossRef] [PubMed]
40. Quidant, R.; Petrov, D.; Badenes, G. Radiation forces on a Rayleigh dielectric sphere in a patterned optical near field. *Opt. Lett.* **2005**, *30*, 1009–1011, doi:10.1364/OL.30.001009. [CrossRef] [PubMed]

41. Volpe, G.; Quidant, R.; Badenes, G.; Petrov, D. Surface plasmon radiation forces. *Phys. Rev. Lett.* **2006**, *96*, 238101, doi:10.1103/PhysRevLett.96.238101. [CrossRef]
42. Kretschmann, E.; Raether, H. Radiative Decay of Non Radiative Surface plasmons excited by light. *Naturforsch* **1968**, *23A*, 2135–2136. [CrossRef]
43. Otto, A. Excitation of nonradiative surface plasma waves in silver by the method of frustrated total reflection. *Zeitschrift für Physik A Hadrons and Nuclei* **1968**, *216*, 398–410, doi:10.1007/BF01391532. [CrossRef]
44. Maier, S.A. *Plasmonics: Fundamentals and Applications*; Springer: New York, NY, USA, 2007. doi:10.1007/0-387-37825-1. [CrossRef]
45. Grigorenko, A.N.; Roberts, N.W.; Dickinson, M.R.; Zhang, Y. Nanometric optical tweezers based on nanostructured substrates. *Nat. Photonics* **2008**, *2*, 365, doi:10.1038/nphoton.2008.78. [CrossRef]
46. Righini, M.; Ghenuche, P.; Cherukulappurath, S.; Myroshnychenko, V.; García de Abajo, F.J.; Quidant, R. Nano-optical trapping of Rayleigh particles and Escherichia coli bacteria with resonant optical antennas. *Nano Lett.* **2009**, *9*, 3387–3391, doi:10.1021/nl803677x. [CrossRef]
47. Chen, C.; Juan, M.L.; Li, Y.; Maes, G.; Borghs, G.; Van Dorpe, P.; Quidant, R. Enhanced optical trapping and arrangement of nano-objects in a plasmonic nanocavity. *Nano Lett.* **2012**, *12*, 125–132, doi:10.1021/nl2031458. [CrossRef]
48. Pang, Y.; Gordon, R. Optical trapping of a single protein. *Nano Lett.* **2012**, *12*, 402–406, doi:10.1021/nl203719v. [CrossRef] [PubMed]
49. Han, X.; Truong, V.G.; Thomas, P.S.; Nic Chormaic, S. Sequential trapping of single nanoparticles using a gold plasmonic nanohole array. *Photonics Res.* **2018**, *6*, 981–986, doi:10.1364/PRJ.6.000981. [CrossRef]
50. Roxworthy, B.J.; Bhuiya, A.M.; Vanka, S.P.; Toussaint, K.C. Understanding and controlling plasmon-induced convection. *Nat. Commun.* **2014**, *5*, 3173, doi:10.1038/ncomms4173. [CrossRef] [PubMed]
51. Wang, K.; Crozier, K.B. Plasmonic trapping with a gold nanopillar. *Chemphyschem* **2012**, *13*, 2639–2648, doi:10.1002/cphc.201200121. [CrossRef]
52. Wang, K.; Schonbrun, E.; Steinvurzel, P.; Crozier, K.B. Trapping and rotating nanoparticles using a plasmonic nano-tweezer with an integrated heat sink. *Nat. Commun.* **2011**, *2*, 469, doi:10.1038/ncomms1480. [CrossRef]
53. Roxworthy, B.J.; Toussaint, K.C. Plasmonic nanotweezers: strong influence of adhesion layer and nanostructure orientation on trapping performance. *Opt. Express* **2012**, *20*, 9591–9603, doi:10.1364/OE.20.009591. [CrossRef]
54. Juan, M.L.; Gordon, R.; Pang, Y.; Eftekhari, F.; Quidant, R. Self-induced back-action optical trapping of dielectric nanoparticles. *Nat. Phys.* **2009**, *5*, 915–919, doi:10.1038/nphys1422. [CrossRef]
55. Bethe, H.A. Theory of diffraction by small holes. *Phys. Rev.* **1944**, *66*, 163–182, doi:10.1103/PhysRev.66.163. [CrossRef]
56. Ebbesen, T.W.; Lezec, H.J.; Ghaemi, H.F.; Thio, T.; Wolff, P.A. Extraordinary optical transmission through sub-wavelength hole arrays. *Nature* **1998**, *391*, 667, doi:10.1038/35570. [CrossRef]
57. Martín-Moreno, L.; García-Vidal, F.J.; Lezec, H.J.; Pellerin, K.M.; Thio, T.; Pendry, J.B.; Ebbesen, T.W. Theory of extraordinary optical transmission through subwavelength hole arrays. *Phys. Rev. Lett.* **2001**, *86*, 1114–1117, doi:10.1103/PhysRevLett.86.1114. [CrossRef]
58. de Abajo, F.J.G. Light transmission through a single cylindrical hole in a metallic film. *Opt. Express* **2002**, *10*, 1475–1484, doi:10.1364/OE.10.001475. [CrossRef] [PubMed]
59. Genet, C.; Ebbesen, T.W. Light in tiny holes. *Nature* **2007**, *445*, 39–46, doi:10.1038/nature05350. [CrossRef] [PubMed]
60. Mestres, P.; Berthelot, J.; Acimovic, S.S.; Quidant, R. Unraveling the optomechanical nature of plasmonic trapping. *Light. Sci. Appl.* **2016**, *5*, e16092, doi:10.1038/lsa.2016.92. [CrossRef] [PubMed]
61. Sainidou, R.; García de Abajo, F.J. Optically tunable surfaces with trapped particles in microcavities. *Phys. Rev. Lett.* **2008**, *101*, 136802, doi:10.1103/PhysRevLett.101.136802. [CrossRef] [PubMed]
62. Neumeier, L.; Quidant, R.; Chang, D.E. Self-induced back-action optical trapping in nanophotonic systems. *New J. Phys.* **2015**, *17*, 123008, doi:10.1088/1367-2630/17/12/123008. [CrossRef]
63. Svoboda, K.; Block, S.M. Biological applications of optical forces. *Biophys. Biomol. Struct.* **1994**, *23*, 247–285. [CrossRef]
64. Bui, A.A.M.; Stilgoe, A.B.; Lenton, I.C.D.; Gibson, L.J.; Kashchuk, A.V.; Zhang, S.; Rubinsztein-Dunlop, H.; Nieminen, T.A. Theory and practice of simulation of optical tweezers. *J. Quant. Spectrosc. Radiat. Transf.* **2017**, *195*, 66–75, doi:10.1016/j.jqsrt.2016.12.026. [CrossRef]

65. Romero-Isart, O.; Juan, M.L.; Quidant, R.; Cirac, J.I. Toward quantum superposition of living organisms. *New J. Phys.* **2010**, *12*, doi:10.1088/1367-2630/12/3/033015. [CrossRef]
66. Descharmes, N.; Dharanipathy, U.P.; Diao, Z.; Tonin, M.; Houdre, R. Observation of backaction and self-induced trapping in a planar hollow photonic crystal cavity. *Phys. Rev. Lett.* **2013**, *110*, 123601, doi:10.1103/PhysRevLett.110.123601. [CrossRef]
67. Bowman, R.W.; Padgett, M.J. Optical trapping and binding. *Rep. Prog. Phys.* **2013**, *76*, 026401, doi:10.1088/0034-4885/76/2/026401. [CrossRef]
68. Stevenson, D.J.; Gunn-Moore, F.; Dholakia, K. Light forces the pace: optical manipulation for biophotonics. *J. Biomed. Opt.* **2010**, *15*, 041503, doi:10.1117/1.3475958. [CrossRef] [PubMed]
69. Capitanio, M.; Pavone, F.S. Interrogating biology with force: single molecule high-resolution measurements with optical tweezers. *Biophys. J.* **2013**, *105*, 1293–1303, doi:10.1016/j.bpj.2013.08.007. [CrossRef] [PubMed]
70. Nussenzveig, H.M. Cell membrane biophysics with optical tweezers. *Eur. Biophys. J.* **2018**, *47*, 499–514, doi:10.1007/s00249-017-1268-9. [CrossRef] [PubMed]
71. Sugiyama, T.; Yuyama, K.I.; Masuhara, H. Laser trapping chemistry : From polymer assembly to amino acid crystallization. *Acc. Chem. Res.* **2012**, *45*, 1946–1954. [CrossRef]
72. Snook, R.D.; Harvey, T.J.; Correia Faria, E.; Gardner, P. Raman tweezers and their application to the study of singly trapped eukaryotic cells. *Integr. Biol. (Camb.)* **2009**, *1*, 43–52, doi:10.1039/b815253e. [CrossRef] [PubMed]
73. Chan, J.W. Recent advances in laser tweezers Raman spectroscopy (LTRS) for label-free analysis of single cells. *J. Biophotonics* **2013**, *6*, 36–48, doi:10.1002/jbio.201200143. [CrossRef]
74. Gillibert, R.; Balakrishnan, G.; Deshoules, Q.; Tardivel, M.; Magazzù, A.; Donato, M.G.; Maragò, O.M.; Lamy de La Chapelle, M.; Colas, F.; Lagarde, F.; et al. Raman tweezers for small microplastics and nanoplastics identification in seawater. *Environ. Sci. Technol.* **2019**, *53*, 9003–9013, doi:10.1021/acs.est.9b03105. [CrossRef]
75. Gieseler, J.; Deutsch, B.; Quidant, R.; Novotny, L. Subkelvin parametric feedback cooling of a laser-trapped nanoparticle. *Phys. Rev. Lett.* **2012**, *109*, 103603, doi:10.1103/PhysRevLett.109.103603. [CrossRef]
76. Li, T.; Kheifets, S.; Raizen, M.G. Millikelvin cooling of an optically trapped microsphere in vacuum. *Nat. Phys.* **2011**, *7*, 527–530, doi:10.1038/nphys1952. [CrossRef]
77. Delić, U.; Reisenbauer, M.; Dare, K.; Grass, D.; Vuletić, V.; Kiesel, N.; Aspelmeyer, M. Cooling of a levitated nanoparticle to the motional quantum ground state. *Science* **2020**, doi:10.1126/science.aba3993. [CrossRef]